

# Environmental Science Nano

Volume 7  
Number 6  
June 2020  
Pages 1621–1856

rsc.li/es-nano



ISSN 2051-8153

**PAPER**

Zongbo Shi *et al.*

Development and application of a ratiometric nanosensor for measuring pH inside the gastrointestinal tract of zooplankton



Cite this: *Environ. Sci.: Nano*, 2020, 7, 1652

## Development and application of a ratiometric nanosensor for measuring pH inside the gastrointestinal tract of zooplankton†

Adam Davis,<sup>‡a</sup> Fatima Nasser,<sup>a</sup> Jamie R. Lead<sup>b</sup> and Zongbo Shi <sup>\*a</sup>

The pH within the gastrointestinal (GI) tract of zooplankton regulates the bioavailability of nutrients and inorganic toxins (metals, nanoparticles) and the breakdown of ingested food. However, measuring the spatial distribution of pH in the GI tract of zooplankton is challenging because the size of the GI tract is extremely small and its micro-environment is complex. Here, we developed a silica-doped ratiometric nanosensor capable of mapping pH in the whole GI tracts of zooplankton. The nanosensors,  $79.0 \pm 25.0$  nm in diameter, were prepared by conjugating pH sensitive dye – fluorescein 5-isothiocyanate and pH insensitive dye (as a reference) – Rhodamine B, to an inert silica nanoparticle. The new nanosensors have a pH sensing range from 5 to 8 which is suitable for determining the pH of the gastrointestinal tract of microorganisms. To demonstrate the application of the nanosensors, we fed them to a model organism *Daphnia magna* neonates to map the pH inside their GI tracts. The results show that the pH was 5.5–6.0 at the anterior section of the GI tract and up to 7.2 in the posterior section. Overall, the pH within the *D. magna* GI tract was significantly lower than the surrounding aqueous medium (pH = 7.8). This indicates that *D. magna* neonates are able to regulate their internal pH. Such a low pH in the anterior part of the GI tract of *D. magna* can increase the solubility of nutrients (e.g., iron oxides) or toxins (e.g., silver nanoparticles) by orders of magnitude, providing a potentially important source of soluble nutrients and/or toxins in surface waters.

Received 15th November 2019,  
Accepted 3rd May 2020

DOI: 10.1039/c9en01300h

rsc.li/es-nano

### Environmental significance

One of the most important parameters in environmental chemistry is the pH. This is widely measured for understanding environmental and biological behaviour and processes, which are usually highly dependent on pH. Measuring pH in a microenvironment or inside aquatic microorganisms is highly challenging because traditional methods either do not work or are very complicated for wide use. In this study, we developed a ratiometric nanosensor that can be used to measure the pH in microenvironments or inside the gastrointestinal tract of zooplankton. The nanosensors were characterized with multiple methods and calibrated before being applied to map the pH of the gastrointestinal tract of a typical zooplankton (*Daphnia magna*). We showed that the pH in the anterior gut is more than 2 pH units lower than the cultural medium. This suggests that zooplankton are able to reduce their internal pH which can increase the solubility of environmental and engineered particles such as iron nanoparticles by orders of magnitude. This process can produce more nutrients such as iron and phosphorus for the aquatic ecosystems but may also generate more soluble toxic metals such as silver to microorganisms.

## 1. Introduction

Zooplankton are key components of aquatic ecosystems, forming the basis of aquatic food webs. They graze on

phytoplankton, which directly regulate the carbon cycle. They also ingest lithogenic particles from aeolian dust deposition, which have the potential to increase the amount of metals and phosphorus to fertilize the oceans.<sup>1</sup> This is because the solubility of metals such as iron and phosphorus is highly pH dependent.<sup>2–5</sup> In addition, the functioning of zooplankton (e.g., breakdown of carbonate and protein) and their role in biogeochemical cycling and toxicity of metals and their nanoparticles are dependent on the pH inside the digestive system of zooplankton.

The determination of pH in aqueous solutions is a frequently performed laboratory procedure and is typically

<sup>a</sup> School of Geography, Earth and Environmental Sciences, The University of Birmingham, Birmingham, UK. E-mail: z.shi@bham.ac.uk;

Tel: +44 (0)1214 149128

<sup>b</sup> Arnold School of Public Health, University of South Carolina, USA

† Electronic supplementary information (ESI) available. See DOI: 10.1039/c9en01300h

‡ Now at Department of Chemistry, Imperial College London, London, UK.



done using a glass electrode. This however cannot be applied to determine the pH inside microorganisms. Microinjection techniques using a pH-sensitive dye was applied by Pond *et al.*<sup>6</sup> to determine the pH in GI tract of *Calanus helgolandicus*. Their results showed a high pH in the hindgut than foregut, which is also shown in *Calanus hyperboreus* by Tang *et al.*<sup>7</sup> by using a microelectrode. However, the measured pH at the foregut is significantly higher in the Pond *et al.*<sup>6</sup> study than that in the Tang *et al.*<sup>7</sup> study, which recorded a pH as low as 5.4. Hasler *et al.*<sup>8</sup> fed *Daphnia magna* with indicators neutral red and bromocresol-phenol to estimate the pH in the alimentary tract from 6.8 in the anterior end and 7.2 at the caudal end. Ebert<sup>9</sup> claimed that the pH of *Daphnia* is 6 to 6.8 in the anterior part of the midgut and 6.6 to 7.2 in the posterior part but it is not clear how this was measured. The microelectrode method is extremely arduous, while microinjection or direct dye feeding methods is subject to uncertainties due to photo-bleaching, solvatochromic shift and/or low fluorescent efficiency.<sup>10</sup>

Materials and methods for producing pH sensors have improved and expanded immensely since this early determination of *Daphnia* GI tract pH.<sup>11,12</sup> The use of fluorescent indicators (rather than absorbance-based) significantly increase the sensitivity of the technique. An aggregation-induced emission (AIE)-based pH sensitive dye – tetraphenylethene-cyanine adduct (TPE-Cy) has the potential to measure intracellular pH.<sup>13,14</sup> An alternative approach to AIE-based sensor is to encapsulate the dyes within an inert matrix (*i.e.* silica) which has numerous benefits: reducing dye interaction with biomolecules,<sup>15</sup> avoiding dye leaking into cellular compartments and allowing reference dyes to be incorporated (for ratiometric measurement).<sup>16</sup> Several nanosensors with fluorescent indicator molecules were developed to detect the pH in microenvironments, particularly intracellular pH in biological cells. The majority of pH nanosensors applications currently in the literature have been demonstrated in mammalian cell lines and associated organelles.<sup>17–20</sup> Studies within *C. elegans* have shown the utility of pH nanosensors in mapping the pH distribution within the entire GI tract of an organism. This study found that pH within the *C. elegans* GI tract varies from 5.96 in the pharynx to 3.59 in the intestine.<sup>21</sup> The application of digital microphotography has also significantly facilitated the application of sensing within biological organisms, allowing images to be taken and later quantitatively analysed.

The aim of this work is to develop functional pH nanosensors based on commercially available fluorescent dyes and apply them to map the pH in the GI tract of a model organism *D. magna*, which is well recognized as sensitive sentinel species in freshwater ecosystems.<sup>22</sup> The developed nanosensors were characterized by a number of analytical techniques and calibrated in normal pH solutions as well as the media used for culturing the *D. magna*. By feeding the *D. magna* with the pH nanosensors, we mapped the pH inside the whole GI tract of individual *D. magna*. The environmental implications of the observed low pH inside the GI tract of the zooplankton are also discussed.

## 2. Materials and methods

### 2.1 Organic modification of fluorescent pH indicator and reference dyes

To facilitate the synthesis of organically modified silica gels it is first necessary to modify commercially available fluorescent dyes to include an alkoxy silane moiety. The alkoxy silane moiety undergoes hydrolysis during silica gel synthesis, forming a covalent bond between the fluorescent dye and silica gel. The chemical modification is achieved through the reaction of the fluorescent dyes with the silanising agent (3-aminopropyl)triethoxysilane (APTS). To help ensure all dye molecules are covalently bound within the silica matrix, APTS is added in excess relative to the fluorescent dyes. All glassware used had been washed using 0.5 M sodium hydroxide for 24 h, in order to remove surface bound silica, then rinsed thoroughly with ultrapure water (MilliQ, 18.2 M $\Omega$ ) and neutralised in ultrapure water for 24 h prior to air drying.

A pH sensitive dye – fluorescein 5-isothiocyanate (FITC),<sup>23</sup> and a pH insensitive reference dye-Rhodamine B (RB)<sup>24,25</sup> were purchased from Sigma Aldrich. FITC is pH dependent because it is able to form a lactone ring when protonated in acidic conditions which quenches its fluorescence and then goes on to form a cation which is also non-fluorescent. Alkoxy silane derivatives of FITC were prepared using a modified method by Wirmsberger *et al.*<sup>26</sup> Depending on the desired final concentration in the silica gel, up to 6.5 mg FITC was dissolved in 20 mL of absolute ethanol (EtOH). Under vigorous stirring, 10  $\mu$ L of APTS was then added and the solution allowed to react at room temperature for three hours in the dark.

A silica compatible derivative of RB was produced using a modified version of the method described by Nedelčev *et al.*<sup>27</sup> RB (0.002 mol, 0.96 g) was dissolved in chloroform (30 mL) and solution stirred and heated to the boiling point of chloroform (61 °C). APTS (2 mM, 0.465 mL) was then added dropwise to the RB solution whilst continuing stirring. The reaction was allowed to continue for 30 min during this time; evaporated chloroform and water formed during the reaction were collected *via* distillation apparatus. After 30 min, any remaining chloroform was removed using vacuum distillation to yield a red/purple solid of RB-APTS.

### 2.2 pH nanosensor fabrication

To produce the pH nanosensors, we firstly generated sol-gel with pH sensitive and insensitive dyes. The silica sol gels were prepared by transferring 20 mL of solution with an alkoxy silane modified dye into a 150 mL round bottom flask, which was then stirred vigorously. To the resulting turbid mixture, 1.6 mL of ultrapure water is added followed by 250  $\mu$ L of 2 M hydrochloric acid (HCl) and 9 mL of approx. 1 g mL<sup>-1</sup> tetraethyl orthosilicate (TEOS). The 2 M HCl was necessary to catalyse the reaction and would have hydrolysed either way in both basic and acidic conditions equally. An advantage of our method was we produced high concentrations of silica nanosensors as acids are





generally used for gel formation. The final reaction mixture was then refluxed for 1 h and once finished the sol was allowed to cool to room temperature before casting to form gels.

To produce pH nanosensors, solutions of dye-APTS conjugates were combined prior to silica gel synthesis or silica sols containing one fluorescent dye were combined prior to casting. The FITC-RB samples were prepared at two concentrations, 0.3 and 3%, by diluting the appropriate amount of nanosensor suspension in 50 mL of ultrapure water. No sonication or vortex step was required.

### 2.3 Characterisation of the nanosensors

The nanosensor preparation method was firstly optimized to produce a stable nanosensor suspension and then characterized by a multi-method approach to establish the nanosensor size, morphology and internal structure.<sup>28</sup> A detailed description of the methods are given in ESI†

### 2.4 *Daphnia magna* incubation

*Daphnia* are freshwater planktonic crustaceans of the order *Cladocera*.<sup>9</sup> *Daphnia* have short reproduction cycles (neonates released every two days). All neonates released are genetically identical with no genetic variation. It has been demonstrated that *D. magna* can ingest particles significantly smaller than 1  $\mu\text{m}$ , including manufactured nanoparticles.<sup>29,30</sup> The *Daphnia magna* used here were of the Bham2 strain and cultured in HH Combo medium (see ESI† text and Table S1). The *Daphnia* cultures were comprised of 15 adult individuals in 900 mL of high hardness (HH) Combo medium and maintained under a light:dark cycle (16:8 h) with a constant temperature of 20  $^{\circ}\text{C} \pm 1$ .

The *Daphnia* GI tract is more or less tubular with three parts: esophagus, midgut, and hindgut (Fig. S1†). There are two small digestive ceca (diverticula) that can be found in the head section of the midgut. The midgut is lined with an epithelium and bears microvilli. Peristaltic contractions of the GI tract wall pass food through the tract, but a peritrophic membrane contains the food and prevents it from entering the ceca. Epithelial cells do not phagocytose particles but absorb molecules.<sup>9</sup> Food is expelled from the hindgut by peristaltic movement but also requires the pressure of more recently acquired food particles. *Daphnia* feeding on green algae are transparent with a tint of green or yellow.

The HH Combo medium of the *D. magna* cultures was refreshed on a weekly basis. Adult individuals were transferred to the new media whilst the neonate *Daphnia* were filtered out for experimental use. The cultures were maintained with the addition of the algal food source *Chlorella vulgaris* once daily (1.5 mL per day). *Chlorella vulgaris* was cultured from the stocks, which were maintained with constant aeration and exposure to UV light. To prepare the algal feed for *D. magna*, the algae stock was centrifuged at 3500 rpm for 15 min. The resulting pellet was then re-suspended in media. To ensure constant cell density in the algal feed the volume of media used to re-

suspend the pellet was adjusted to ensure an optical density of 0.8, which was determined using the absorbance of the suspension at 440 nm.

### 2.5 Calibration of pH nanosensors

Firstly, pH buffer of moderate ionic strength and wide pH range was prepared to calibrate the pH nanosensors. Sodium phosphate/citric acid pH buffer was chosen and prepared between pH 2.5 and 8.0 in 0.5 pH unit intervals. Standard solutions of 250 mL 2 M sodium phosphate dibasic and 250 mL 0.1 M citric acid were prepared in acid washed glassware. To prepare each 20 mL of buffer appropriate quantities of the two standard solutions were added together as shown in Table S2† and then diluted to 40 mL with ultrapure water.

To calibrate the pH nanosensors using pH buffers, 20  $\mu\text{L}$  of 3% nanosensor suspension was placed into each well of a microplate and diluted in pH buffer to 100  $\mu\text{L}$ . The microplates were then read using the optical microplate reader. The microplates are analysed by scanning across each individual well in two coordinates. The fluorescence well plate measurements were made using a BMG Labtech FLUOstar Omega, a filter-based multi-mode plate reader. Filter sets used for each dye are recorded. The excitation emission wavelengths of filter sets used with FLUOstar Omega plate reader for FITC are 485 nm and 520 nm, and 544 nm and 580 nm.

The nanosensors are also calibrated in the HH Combo media.

### 2.6 pH measurements

Measurements of pH were made using FITC RB-doped silica nanosensors within *D. magna* neonates (age <48 h). Prior to the imaging experiments the *D. magna* neonates were incubated in 0.3% (3% mortality) nanosensors suspension (made up in HH Combo medium) for 18 h, in the dark at room temperature (20  $^{\circ}\text{C}$ ). The exposures were made in a 12-well plate (Costar) with a maximum of 10 neonates in 4 mL for each well.

Laser scanning confocal microscopy (LSCM) imaging was performed using the Zeiss LSM 710 ConfoCor 3 equipped with 458, 488, and 514 nm argon laser lines as well as 543 and 633 nm HeNe diode lasers. The pH maps within the GI tract of the *D. magna* were obtained with the live neonates placed within a 35 mm plain glass bottom dish and again using the 10 $\times$  objective lens. The *Daphnia* were exposed to FITC RB for 24 h in the absence of algae prior to measurement. The FITC RB nanosensors were excited using the 488 and 543 nm laser lines respectively. In addition to the fluorescence images, a transmitted light image was also recorded. To adequately capture the motion of the *D. magna* the resolution of the images was decreased to 512  $\times$  512 pixels and the frame rate increased to maximum.

All image processing and analyses were conducted using the open source software ImageJ/FIJI. In the first instance calibration images were taken of nanosensors in various pH



buffers as well as in HH Combo medium adjusted to different pH values. Using the ImageJ 'measure' function the intensity of both the green and red channels were obtained and a ratio for each known pH calculated. A pH calibration curve in both pH buffers and in pH adjusted media was then generated. During pH measurements within *D. magna* along with internal calibration, the region of interest (ROI) was first located using the ImageJ selection tools. Pixel values outside the ROI were converted to 'not a number' (NaN) to exclude them from further analysis. The ROI was then averaged using a median filter (2 pixels). The channels of the images were subsequently separated and a ratio of the green and red channels obtained using the ImageJ 'image calculator' function. A 16 colour look-up table (LUT) was then applied to the image to convert the image containing ratio values into a 'heat-map'. The 'calibration' function was used to apply the external calibration curve to the image and therefore convert the ratio values to pH values. A corresponding calibration bar and a scale bar were then added using the respective ImageJ functions.

### 3. Results and discussions

#### 3.1 Physical characteristics of the pH nanosensors

A summary of the FITC RB nanosensor characterisation data is provided in Table 1. The average hydrodynamic diameter (*z* average) of the three batches of nanosensors measured by dynamic light scattering (DLS) (F-RB *x*, F-RB *y* and F-RB *z*) is 109.6 nm with a polydispersity index (pdi) of 0.107. The nanosensors remained stable after 24 h (*z* average 110.5 nm with a pdi of 0.120) and 120 h (*z* average of 111.8 nm with a pdi of 0.141) of preparation (Fig. S2 and S3; Table S3†).

Zeta potential measured on the nanosensors at 0.3% by DLS is shown in Table S4.† The average zeta potential measured for the FITC RB nanosensors was  $-4.2$  mV with a deviation of 6.43 mV. A slightly negative zeta potential at neutral to mildly acidic pH is expected of the FITC RB nanosensors as both the silica particle hydroxyl groups and FITC indicator on the particle surface are primarily still protonated, with some anions. The FITC RB nanosensors (3%) has positive zeta potentials at  $12.9 \pm 9.35$  mV. This is fairly low, with  $> \pm 25$  mV usually required to provide adequate colloidal stability in a charge stabilised system. Given the low zeta potential, it is therefore likely that the FITC RB nanosensors are mainly dispersed. The particles appear stable (Table 2), suggesting it does not have a critical role in providing steric hindrance to particle aggregation.

**Table 1** Summary of multi-method size measurements for FITC RB-doped silica nanoparticles

Technique	Nanosensor size/nm	Type of diameter measured physical parameter
DLS	$109.6 \pm 9.0$	Hydrodynamic diameter
DCS	$84.9 \pm 4.8$	Equivalent spherical volume
TEM	$79.0 \pm 25.0$	Diameter

**Table 2** Summary of DLS results for FITC RB nanosensors in HH Combo medium over 24 h

Sample	Z average/d.nm	pdi	Count rate/kcps
F-RB <i>x</i> 0 h	112	0.075	346.3
F-RB <i>x</i> 1 h	111.4	0.068	365.8
F-RB <i>x</i> 24 h	114	0.135	458.9
F-RB <i>y</i> 0 h	107.4	0.092	321.5
F-RB <i>y</i> 1 h	106.3	0.083	346.3
F-RB <i>y</i> 24 h	110	0.155	444.6
F-RB <i>z</i> 0 h	116.1	0.082	357
F-RB <i>z</i> 1 h	114.3	0.102	367.4
F-RB <i>z</i> 24 h	117.9	0.156	479.5

Considering the absence of polymer or macromolecules, it is likely that it is the presence of the organic dyes on the particle surface which provide most of the steric interactions.

The diameter of the FITC RB (F-RB *x*) estimated from equivalent spherical volume by DCS (differential centrifugal sedimentation) was 84.9 nm with a peak width of 54.0 nm (Fig. S4†). As measured using DCS, the diameter of F-RB *y* was 80.3 nm with a peak width of 51.8 nm and that of the sample F-RB *z* 89.8 nm with a peak width of 59.5 nm (data not shown). On average the FITC RB nanosensor diameter as measured by DCS was around 25 nm lower than when measured using DLS. This is not surprising given the tendency of DLS to overestimate particle size, due a bias towards larger particles which scatter more light compared with smaller particles.<sup>28</sup>

Transmission electron microscopy (TEM) images of the FITC RB-doped silica nanoparticles were initially used to provide another measure of nanoparticle core diameter. Typical images used for the particle size analysis are shown in Fig. S5.†

At higher magnification the lower density structures within the FITC-RB doped silica nanoparticles can be seen (Fig. 1). In

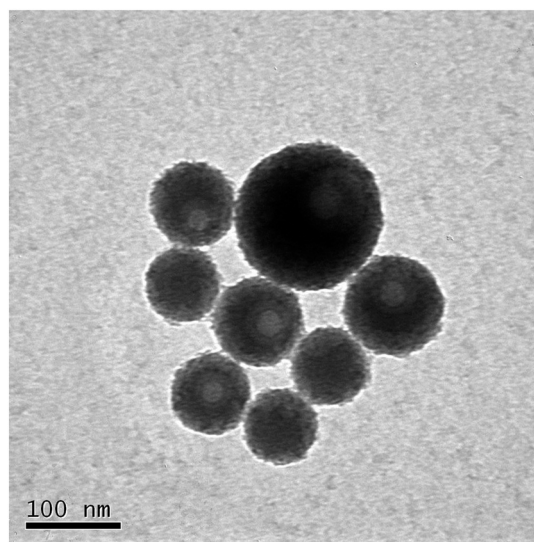


**Fig. 1** Higher magnification TEM images of FITC RB-doped silica nanoparticles.



the TEM images, materials of low density *i.e.* carbon interfere less with the path of the electron beam and therefore appear less dark. In comparison, unlabelled silica nanoparticles do not show a less dark and lower density cores (Fig. S6†) Subsequent re-analysis and separation based upon particle type (silica and secondary particles, presumed carbon) yielded a revised estimation of the FITC RB-doped SiNP mean diameter of 79 nm  $\pm$  25 nm. The core-shell structure of the pH nanosensors (Fig. 1) has several advantageous properties over free-dye probes during biological imaging. The main advantages include prevention of the sensing component from interacting with potentially interfering species (while allowing H<sup>+</sup> diffusion) in the intracellular environment and reducing the potential for toxic effects from the sensing material to the microorganisms.<sup>15</sup> Additionally, silica nanoparticles with core-shell architecture have been found to have enhanced properties including reduced photo-bleaching, minimized solvatochromic shift and increased fluorescent efficiency relative to free dye in aqueous solution.<sup>10</sup>

The relatively high ionic strength of HH Combo medium has the potential to shield nanoparticle surface charge, reducing stabilisation and resulting in nanosensor aggregation. Therefore, prior to exposure of *D. magna* to the pH nanosensors, we firstly measured the stability of the nanosensors when suspended in *D. magna* culture medium (HH Combo). DLS measurements (Fig. S7†) showed that over a 24 h exposure period the FITC RB-doped SiNPs remain relatively stable in the HH Combo medium (Table 2). A small decrease in peak intensity can be seen when comparing time points with the lowest intensity at 24 h as may be associated with a broadening of the particle size distribution.

The stability data reported here further supported the argument above that the majority of the particle stability was provided from steric hindrance rather than electrostatic charge. We undertook further work using the same synthesis methods but not containing any organic dyes. The average diameter of these unlabelled nanoparticles was significantly larger at 495 nm  $\pm$  107 nm (measured by TEM) which further confirmed that the steric interactions between the organic dyes provided stability with smaller nanoparticles. Despite the relatively high ionic strength found in the HH Combo medium, the FITC RB nanosensors remain remarkably stable. If indeed the particles were charge stabilised it would be expected that the charge on the particles is neutralized/shielded by the excess of ions in the medium, leading to significant aggregation of the particles. The individual DLS results for FITC RB nanosensors in HH Combo medium can be found in Table 2.

*D. magna* neonates excrete and shed a complex mixture of organic material such as proteins and carbohydrates into their media. The release of these materials is known as 'conditioning the medium'.<sup>31</sup> These released biomolecules have the potential to interact and adsorb to the surface of the nanosensors creating a corona which is well known to influence the stability of the particles in the medium.

To understand if indeed this was the case, the stability of FITC RB nanosensors was also studied in conditioned medium (*D.*

*magna* for 24 h) over the same 24 h time frame as before. Conditioned HH Combo medium was prepared by placing 10 neonates (1–3 days old) into 5 mL of HH Combo medium for 24 h in the absence of algae. During this time biomolecules released by *Daphnia magna* (*i.e.* excreted proteins) entered into solution, hence 'conditioning' the medium. The results shown in Fig. 2. No significant change can be seen over the course of the first hour of particle incubation in the conditioned medium. A slightly more pronounced change however was found after 24 h with the conditioned medium, than was found with HH Combo medium alone, with some signs of large aggregates being formed (Fig. 2).

During the *D. magna* exposure in which the water fleas were placed in a suspension of FITC RB nanosensors, it was observed that large (visible to the naked eye) aggregates were deposited on the bottom of the exposure container. This was not the case when *D. magna* neonates were absent from the exposure suspension. It therefore appears that the ingestion and subsequent expulsion of the SiNPs had a strong effect upon particle aggregation state.

### 3.2 Uptake of pH nanosensors in *D. magna*

It was found that *D. magna* exposed to a 0.3% solution of FITC RB nanosensors suspended in HH Combo over a 24 h period, were able to ingest enough material to provide high fluorescence intensity signal, when observed using LSCM. It can be seen in Fig. 3 that the nanosensors are retained almost exclusively within the GI tract, with very little extraneous signal from the carapace or internal organs. A washing step was done before imaging so that any particles bound to the external carapace were removed as to only account for particles taken up by filter feeding.

### 3.3 Toxicity of pH nanosensors towards *D. magna*

For efficient uptake of nanosensors into the *D. magna* GI tract a relatively high concentration of nanosensors is desirable. However to achieve a reliable measurement of GI tract pH under normal functioning conditions, it is necessary to avoid concentrations which will induce a toxic effect in the organism of interest or change the pH inside its GI tract. To optimise the concentration of pH nanosensors used, the

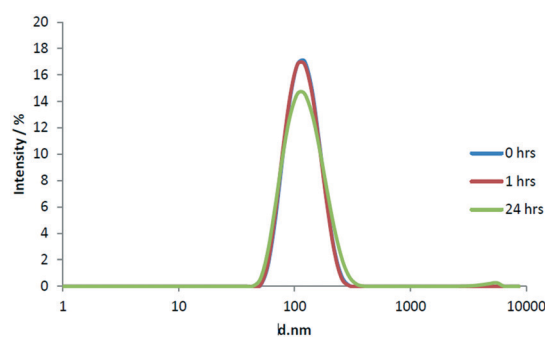
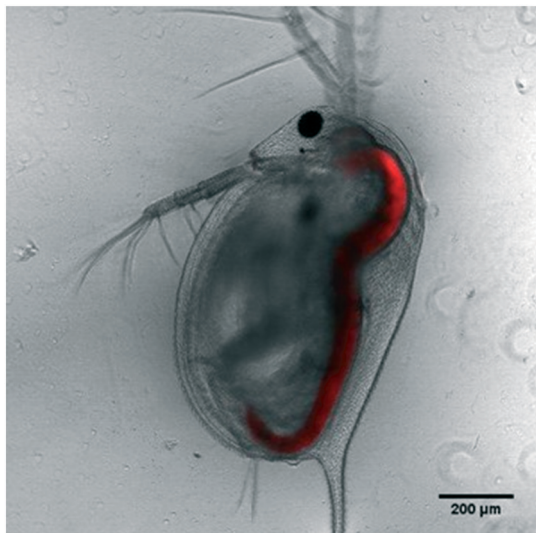


Fig. 2 Average DLS result for FITC RB nanosensors in pre-conditioned HH Combo medium over 24 h.







**Fig. 3** LSCM images of FITC RB nanosensor uptake in *D. magna* – red channel fluorescence superimposed on transmitted brightfield image.

following mortality curve (Fig. S8†) was produced. In the pH measurements, we exposed the *D. magna* to 0.3% diluted stock, at which concentration the mortality rate is very small.

### 3.4 Calibration of pH nanosensors

The modelled  $pK_a$  values for the nanosensor is 6.66. This is reflected in the pH response shown in Fig. S9† in buffer solution. The curve is linear starting at approximately pH 5.0 and reaches a plateau at pH 8.0. The resulting calibration curve in the HH Combo media is shown in Fig. 4. The pH response on the FITC RB nanosensors in HH Combo medium matched well to that produced in the pH buffer calibration with a linear range from approximately pH 5.0 and 8.0 (Fig. S9†).

### 3.5 Measurement of pH within GI tract of *D. magna*

Once the calibration was applied to the fluorescence ratio images, they were combined with transmitted light micrographs of the *D. magna* to produce pH distribution

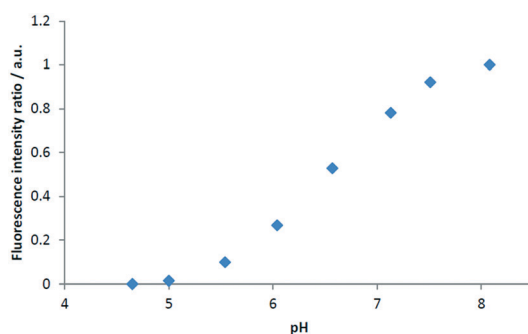


**Fig. 4** FITC RB nanosensors calibration in HH Combo medium, normalised fluorescence intensity ratio of IFITC/IRB with varying pH.

maps within the GI tract. An example pH map is given in Fig. 5. Determining the mean pH of the *D. magna* allowed the external calibration to be modelled and adapted for internal pH measurements.

Within the *D. magna* GI tract the pH appears to lowest at the lining of the intestine at around pH 5.5 with the highest values reaching 7.2. The lowest pH determined here is significantly lower than that measured by Hasler *et al.*<sup>8</sup> using casein with indicators neutral red and bromocresol-phenol, which estimated a pH of 6.8 in the anterior end. The use of fluorescent nanosensors and advanced fluorescence microscopy however, has allowed for a detailed pH distribution map along the *D. magna* GI tract to be generated.

Overall, the pH within the *D. magna* GI tract was found to be maintained at a lower mean pH than that of the surrounding medium at pH 7.8 indicating that *D. magna* neonates are able to regulate their internal pH despite an intake of the surrounding medium at a much higher pH.

Over a time series the boluses of aggregated nanosensors were seen to move through the GI tract of the *Daphnia* with the peristaltic action of the intestine clearly visible. A bolus of material can be seen to be ejected from the *Daphnia* GI tract in image B of Fig. 5. Despite the egress of material through the GI tract, the set pH within the individual intestinal regions (esophagus, midgut, and hindgut) was found to be maintained.

Our results showed that the new nanosensors can be used to measure the pH in a wide range (from 5 to 8) in biological microenvironment, for example, other zooplankton such as krill.

### 3.6 Environmental implications

The low pH within the GI tracts of zooplankton (compared with external pH) such as *D. magna* has important implications for the biogeochemical cycling of elements and toxicity of nanoparticles. For example, the solubility of iron oxides is more than two orders of magnitude higher at pH 5.5 in comparison to 7.8.<sup>2</sup> The solubility of ferrihydrite nanoparticles is  $<10^{-11}$  mol L<sup>-1</sup> at pH 7.8 and  $\sim 10^{-9}$  mol L<sup>-1</sup> at pH 5.5.<sup>2</sup> Therefore, injection of insoluble dust particles by zooplankton could significantly enhance the supply of bioavailable iron to the phytoplankton,<sup>1</sup> which provides soluble (and thus bioavailable) iron *via* the prevailing food web structure to the ocean ecosystems. Barbeau *et al.*<sup>32</sup> also demonstrated that iron colloids otherwise unavailable to phytoplankton, were made bioavailable through digestion in acidic food vacuoles of protozoan grazers and were subsequently released in a more labile form. Metals that are bound to naturally occurring colloids and nano-particulates may also be desorbed at lower pH, making them more soluble and thus bioavailable.

In addition to naturally occurring colloids and nano-particulates, there is increasing input of incidental and manufactured nanomaterials into the environment, arising from the use and disposal of consumer and industrial



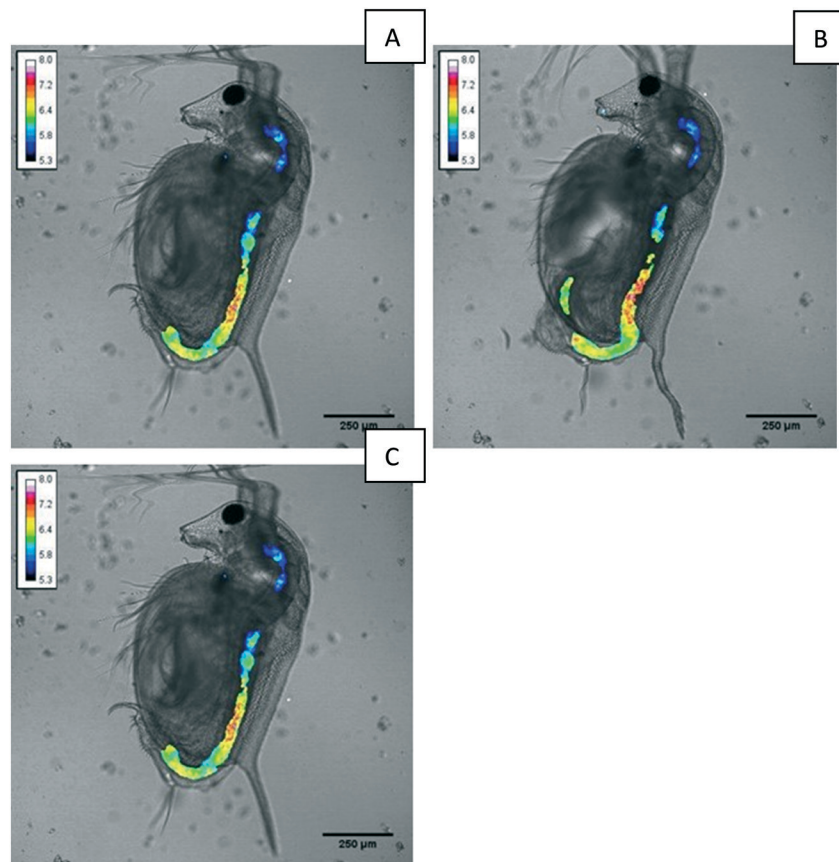


**Fig. 5** Maps of pH within the GI tract of *D. magna*, produced using FITC RB nanosensors, taken from a time series (frame A, B and C at time 0, 2.5 and 5 min approximately) of an individual *Daphnia* suspended in HH Combo medium. After exposure to nanosensors, the individual was taken to the confocal microscope for analysis immediately.

products that contain nanomaterials. Manufactured silver nanoparticles are a prominent example and have been included in a number of consumer products such as clothing and domestic appliances as an anti-microbial agent.<sup>33</sup> Silver in its ionic form is a well known environmental hazard because of its toxic, persistent and potentially bioaccumulative properties.<sup>34,35</sup> The local and internal conditions *i.e.* low pH within the GI tract of aquatic organisms has been shown to be an important factor in dissolving silver nanoparticles<sup>14</sup> and increase their bioavailability (thus toxicity) within the organisms themselves and for other aquatic organisms.<sup>35</sup> The solubility of 5 nm silver nanoparticles is about  $3 \times 10^{-3} \text{ mol L}^{-1}$  at pH 8, which is more than 10 lower than that at pH 5.5.<sup>36</sup> Our results suggest that future nanoparticle solubility and toxicity studies should incorporate an understanding of, and experiments using, the pH conditions in the GI tract of organisms such as *Daphnia*, in addition to the conditions of standard exposure media. Data and knowledge of such conditions will inform a more mechanistic link between transformations and bioavailability of nanoparticles and their toxicity. In addition, these sensors are useful for helping understand sorption-desorption reactions of metals from both inorganic and carbon-based sensors. In all these cases, GI tract conditions

can be mimicked *in vitro* to provide improved understanding before *in vivo* experiments for which can be better interpreted in light of the *in vitro* work.

The lower pH in the GI tract also affects our understanding of carbonate chemistry, because the carbonate is more undersaturated with respect to calcite in the GI tract under the newly established pH conditions. As a result, coccoliths ingested by zooplankton are subject to greater dissolution than previously thought. Development of sensors useful at other pH values will extend the utility of these sensors.

The pH nanosensors developed here have the potential to further our understanding of environmental toxicity. For example, they can be used to investigate the potential variations in the pH in the GI tract of *Daphnia* (and other zooplankton) living in different environments, *e.g.*, different lakes and ponds, and coastal and open ocean. This will help us to understand whether *Daphnia* living in different environments have different susceptibility to stresses such as exposure to nanomaterials. The nanosensors can also be used to determine whether the pH inside the GI tract of *Daphnia* will change in response to environmental stresses, and whether younger *Daphnia* has different GI tract pH distribution than adult or older *Daphnia*. This could help us to identify particularly sensitive developmental stages of a *Daphnia* to environmental stresses.





Therefore, the answers to these questions for *Daphnia* will improve their application as a model for testing chemical toxicity and informing environmental regulations of chemicals.

## 4. Conclusions

In summary, a ratiometric nanosensor has been developed that can be used to measure the pH in microenvironments, including in the guts of microorganisms such as *D. magna*. The nanosensor particles have a mean diameter  $79.0 \pm 25.0$  nm based on TEM analysis. It has a detection range of around 5 to 8. This nanosensor has been applied to detect the pH inside the gastrointestinal tract. The results showed the pH was 5.5–6.0 at the anterior section of the GI tract and up to 7.2 in the posterior section. Overall, the pH within the *D. magna* GI tract was significantly lower than the surrounding aqueous medium (pH = 7.8). pH in the GI tract of other microorganisms might be slightly different but incorporating other pH sensitive dyes can further enhance the pH detection range for wider environmental and biological applications. The synthesis methodology may also be used for developing nanosensors for other environmental parameters as long as their changes cause measurable variations in fluorescent intensity. For example, metal (e.g., zinc), oxygen and redox sensitive fluorescence dyes may be developed as nanosensors for detecting metal ions, oxygen content and redox potential in microenvironments.

## Conflicts of interest

There are no conflicts to declare.

## Acknowledgements

This work is funded by Natural Environment Research Council-Royal Society of Chemistry Technology studentship (NE/J017779/1) and Natural Environment Research Council (NE/I021616/1). We thank Jonathan Aylott from Nottingham University for support during the initial planning of the research; we also thank Eva Valsami-Jones and Christine Elgy for advice and technical support. Thanks are also paid to the two anonymous referees who provided highly valued and constructive comments.

## References

- 1 K. Schmidt, C. Schlosser, A. Atkinson, S. Fielding, H. J. Venables, C. M. Waluda, E. P. Achtererg and E. P. Zooplankton, Gut Passage Mobilizes Lithogenic Iron for Ocean Productivity, *Curr. Biol.*, 2016, **26**, 2667–2673.
- 2 R. M. Cornell and U. Schwertmann, *The Iron Oxides: Structure, Properties, Reactions, Occurrence and Uses*, Wiley-VCH Publishers, New York, 2003.
- 3 A. Stockdale, M. D. Krom, R. J. G. Mortimer, L. G. Benning, K. S. Carslaw, R. Herbert, Z. Shi, S. Myriokefalitakis, M. Kanakidou and A. Nenes, Supply of bioavailable phosphorus to the oceans: understanding the nature of atmospheric acid processing of mineral dusts, *Proc. Natl. Acad. Sci. U. S. A.*, 2016, **113**, 14639–14644, DOI: 10.1073/pnas.1608136113.
- 4 Z. Shi, M. D. Krom, S. Bonneville, A. Baker, T. Jickells and L. G. Benning, Formation of iron nanoparticles and increase in iron reactivity in the mineral dust during simulated cloud processing, *Environ. Sci. Technol.*, 2009, **43**, 6592–6596, DOI: 10.1021/es901294g.
- 5 Z. Shi, M. D. Krom, S. Bonneville and L. G. Benning, Atmospheric processing outside clouds increases soluble iron in mineral dust, *Environ. Sci. Technol.*, 2015, **49**, 1472–1477, DOI: 10.1021/es504623x.
- 6 D. W. Pond, R. P. Harris and C. A. Brownlee, Microinjection technique using a pH-sensitive dye to determine the gut pH of *Calanus helgolandicus*, *Mar. Biol.*, 1995, **123**, 75–79.
- 7 K. W. Tang, R. N. Glud, A. Glud, A. S. Rysgaard and T. G. Nielsen, Copepod guts as biogeochemical hotspots in the sea: Evidence from microelectrode profiling of *Calanus* spp, *Limnol. Oceanogr.*, 2011, **56**, 666–672.
- 8 A. D. Hasler, The physiology of digestion of plankton crustacean: i. some digestive enzymes of daphnia, *Biol. Bull.*, 1935, **68**, 207–214.
- 9 D. Ebert, *Ecology, Epidemiology, and Evolution of Parasitism in Daphnia. Bethesda (MD): National Library of Medicine (US)*, National Center for Biotechnology Information, 2005.
- 10 H. Ow, D. R. Larson, M. Srivastava, B. A. Baird, W. W. Webb and U. Wiesner, Bright and Stable Core–Shell Fluorescent Silica Nanoparticles, *Nano Lett.*, 2005, **5**, 113–117.
- 11 O. S. Wolfbeis, Materials for fluorescence-based optical chemical sensors, *J. Mater. Chem.*, 2005, **15**, 2657–2669.
- 12 O. S. Wolfbeis, An overview of nanoparticles commonly used in fluorescent bioimaging, *Chem. Soc. Rev.*, 2015, **44**, 4743–4768.
- 13 S. Chen, Y. Hong, Y. Liu, J. Liu, J. C. W. T. Leung, M. Li, R. T. K. Kwok, E. Zhao, J. W. Y. Lam, Y. Yu and B. Z. Tang, Full-Range Intracellular pH Sensing by an Aggregation-Induced Emission-Active Two-Channel Ratiometric Fluorogen, *J. Am. Chem. Soc.*, 2013, **135**, 4926–4929.
- 14 N. Yan, B. Z. Tang and W. X. Wang, In Vivo Bioimaging of Silver Nanoparticle Dissolution in the Gut Environment of Zooplankton, *ACS Nano*, 2018, **12**, 12212–12223.
- 15 J. W. Aylott, Optical nanosensors—an enabling technology for intracellular measurements, *Analyst*, 2003, **128**, 309–312.
- 16 J. Han and K. Burgess, Fluorescent Indicators for Intracellular pH, *Chem. Rev.*, 2010, **110**, 2709–2728.
- 17 J. Peng, X. He, K. Wang, W. Tan, Y. Wang and Y. Liu, Noninvasive monitoring of intracellular pH change induced by drug stimulation using silica nanoparticle sensors, *Anal. Bioanal. Chem.*, 2007, **388**, 645–654.
- 18 H. Sun, T. L. Andresen, R. V. Benjaminsen and K. Almdal, Polymeric nanosensors for measuring the full dynamic pH range of endosomes and lysosomes in mammalian cells, *J. Biomed. Nanotechnol.*, 2009, **5**, 676–682.
- 19 R. V. Benjaminsen, H. Sun, J. R. Henriksen, N. M. Christensen, K. Almdal and T. L. Andresen, Evaluating Nanoparticle Sensor Design for Intracellular pH Measurements, *ACS Nano*, 2011, **5**, 5864–5873.
- 20 W. Shi, X. Li and H. Ma, A Tunable Ratiometric pH Sensor Based on Carbon Nanodots for the Quantitative



- Measurement of the Intracellular pH of Whole Cells, *Angew. Chem.*, 2012, **124**, 6538–6541.
- 21 V. M. Chauhan, G. Orsi, A. Brown, D. I. Pritchard and W. Aylott, Mapping the Pharyngeal and Intestinal pH of *Caenorhabditis elegans* and Real-Time Luminal pH Oscillations Using Extended Dynamic Range pH-Sensitive Nanosensors, *ACS Nano*, 2013, **7**, 5577–5587.
- 22 J. R. Shaw, M. E. Pfrender, B. D. Eads, R. Klaper, A. Callaghan, R. M. Sibly, I. Colson, B. Jansen, D. Gilbert and J. K. Colbourne, *Daphnia* as an emerging model for toxicological genomics, *Adv. Exp. Biol.*, 2018, **2**, 165–328.
- 23 M. M. Martin and L. Lindqvist, The pH dependence of fluorescein fluorescence, *J. Lumin.*, 1975, **10**, 381–390.
- 24 H. Sun, A. M. Scharff-Poulsen, H. Gu and K. Almdal, Synthesis and Characterization of Ratiometric, pH Sensing Nanoparticles with Covalently Attached Fluorescent Dyes, *Chem. Mater.*, 2006, **18**, 3381–3384.
- 25 S. Hu, L. Sun, M. Liu, H. Zhu, H. Guo and H. Sun, A highly dispersible silica pH nanosensor with expanded measurement ranges, *New J. Chem.*, 2015, **39**, 4568–4574.
- 26 G. Wirnsberger, B. J. Scott and G. D. Stucky, pH Sensing with mesoporous thin films, *Chem. Commun.*, 2001, 119–120.
- 27 T. Nedelčev, D. Račko and I. Krupa, Preparation and characterization of a new derivative of rhodamine B with an alkoxy silane moiety, *Dyes Pigm.*, 2008, **76**, 550–556.
- 28 R. F. Domingos, M. A. Baalousha, Y. Ju-Nam, M. M. Reid, N. Tufenkji, J. R. Lead, G. G. Leppard and K. J. Wilkinson, Characterizing Manufactured Nanoparticles in the Environment: Multimethod Determination of Particle Sizes, *Environ. Sci. Technol.*, 2009, **43**, 7277–7284.
- 29 F. Nasser and I. Lynch, Secreted protein eco-corona mediates uptake and impacts of polystyrene nanoparticles on *Daphnia magna*, *J. Proteomics*, 2015, **30**, 45–51, DOI: 10.1016/j.jprot.2015.09.005.
- 30 B. K. Gaiser, A. Biswas, P. Rosenkranz, M. A. Jepson, J. R. Lead, V. Stone, C. R. Tyler and T. F. Fernandes, Effects of silver and cerium dioxide micro- and nano-sized particles on *Daphnia magna*, *J. Environ. Monit.*, 2011, **13**, 1227–1235.
- 31 A. Albanese and W. C. Chan, Effect of gold nanoparticle aggregation on cell uptake and toxicity, *ACS Nano*, 2011, **5**, 5478–5489.
- 32 K. Barbeau, J. W. Moffett, D. A. Caron, P. L. Croot and D. Erdner, Role of protozoan grazing in relieving iron limitation of phytoplankton, *Nature*, 1996, **380**, 61–64.
- 33 S.-J. Yu, Y. G. Yin and J. F. Liu, Silver nanoparticles in the environment, *Environ. Sci.: Processes Impacts*, 2013, **15**, 78–92.
- 34 S. N. Luoma, Silver nanotechnologies and the environment: old problems and new challenges? Washington DC: Woodrow Wilson International Center for Scholars or The PEW Charitable Trusts, 2008.
- 35 J. Fabrega, S. N. Luoma, C. R. Tyler, T. S. Galloway and J. R. Lead, Silver nanoparticles: Behaviour and effects in the aquatic environment, *Environ. Int.*, 2011, **37**, 517–531.
- 36 B. Molleman and T. Hiemstra, Time, pH, and size dependency of silver nanoparticle dissolution: the road to equilibrium, *Environ. Sci.: Nano*, 2017, **4**, 1314–1327.

